Impact of Bias Correction Methods on Estimation of Soil Moisture When Assimilating Active and Passive Microwave Observations

Alejandro Monsivais-Huertero, *Senior Member, IEEE*, Jasmeet Judge, *Senior Member, IEEE*, Susan Steele-Dunne, and Pang-Wei Liu, *Member, IEEE*

***Abstract*—In this paper, bias correction approaches are investigated to understand their impact on assimilating active and/or passive microwave observations on near-surface soil moisture (SM) estimates. Synthetic and field observations were assimilated in a soil–vegetation–atmosphere transfer model linked with an integrated active–passive model at L-band for bare soil. The two bias correction methods included in this study are the online bias correction with feedback (BCWF) with extended implementation with nonlinear observation operators and the simultaneous state parameter (SSP) update. New equations for BCWF were derived for the case of nonlinear observation operators because current versions of this approach were not applicable for improving SM by assimilating microwave observations. In SSP, the bias is compensated by tunning the values of the parameters. The two approaches resulted in similar accuracy for improving SM estimates compared with the uncorrected estimates. SSP showed the highest certainty for both synthetic and field observations. Using the bias correction methods, the mean estimates of SM improved by up to 88%, 87%, and 94%, when passive, active, and active–passive synthetic observations were assimilated, respectively, compared with the open-loop estimates. In contrast, when assimilating field observations from the Eleventh Microwave Water Energy Balance Experiment, the mean estimates of SM improved by up to 44%, 18%, and 48%, when passive, active, and active–passive observations were assimilated, respectively, compared with open-loop estimates. The decrement in improving the SM estimates suggests sources of uncertainty other than those from model parameters and forcings.**

***Index Terms*—Backscattering coefficient, bias correction, ensemble Kalman filter (EnKF) assimilation, microwave brightness temperature, soil moisture (SM).**

Manuscript received March 30, 2015; accepted June 5, 2015. This work was supported by the National Aeronautics and Space Administration Terrestrial Hydrology Program NNX09AK29G and by the National Council of Science and Technology of Mexico (CB-2010-155375). The work of S. Steele-Dunne was supported by the Netherlands Organisation for Scientific Research (NOW) Veni Grant Program (ALW 863.09.015).

A. Monsivais-Huertero is with the Escuela Superior de Ingeniería Mecánica y Eléctrica Ticomán, Instituto Politecnico Nacional, 07738 Mexico City, DF Mexico (e-mail: monsivais@ufl.edu).

J. Judge and P.-W. Liu are with the Center for Remote Sensing, Department of Agricultural and Biological Engineering, University of Florida, Gainesville, FL 32611 USA.

S. Steele-Dunne is with the Department of Civil Engineering, Delft University of Technology, 2628 Delft, The Netherlands.

Color versions of one or more of the figures in this paper are available online at http://ieeexplore.ieee.org.

Digital Object Identifier 10.1109/TGRS.2015.2455037

I. Introduction

ACCURATE knowledge of soil moisture (SM) is crucial in hydrology, micrometeorology, and agriculture for estimating energy and moisture fluxes at the land surface. Soil–vegetation–atmosphere transfer (SVAT) models are typically used to simulate energy and moisture transport in soil and vegetation [1]. Although SVAT models coupled with vegetation growth models capture the biophysics of dynamic vegetation fairly well, SM estimates still diverge from reality due to errors in computation and uncertainties in model parameters, forcings, and initial conditions. The model estimates of SM can be significantly improved by assimilating remotely sensed observations that are sensitive to SM changes, such as passive observations of brightness temperature T_B and/or active observations of backscattering coefficient σ^0 at frequencies $<$10 GHz [2]–[5]. For SM studies, observations at L-band (1.2–1.4 GHz) are desirable due to their high sensitivity, large penetration depths, and system feasibility. The currently operational European Space Agency Soil Moisture and Ocean Salinity (SMOS) [6] includes a passive system at L-band. In the near future, the National Aeronautics and Space Administration Soil Moisture Active Passive (SMAP) mission will include both active and passive sensors [7].

Over the last decade, significant progress has been made in estimating near-surface SM retrieved from active and/or passive microwave observations in SVAT models (e.g., [2], [3], and [8]–[19]). Although both the active and passive techniques observe radiation quantities that are functions of SM and exhibit similar sensitivities to soil water [20], the high sensitivity of σ^0 to soil surface roughness may produce a much larger dynamic range than that produced due to the effects of changes in soil water alone. This makes it challenging to distinguish between the contributions of soil water in the backscatter signal to obtain absolute soil water estimates. Recently, a few studies have linked the SVAT models with forward microwave models to allow assimilation of microwave observations directly rather than assimilating retrieved near-surface SM obtained from microwave observations (e.g., [2], [21], and [22]).

The active and passive (AP) microwave observations provide complementary information regarding soil and vegetation. Studies that use both AP observations in the SVAT-Microwave models for assimilation are rare and recent. These synthetic studies typically utilize separate formulations for estimating

0196-2892 © 2015 IEEE. Personal use is permitted, but republication/redistribution requires IEEE permission.
See http://www.ieee.org/publications_standards/publications/rights/index.html for more information.

terrain backscatter and emission [22]. Because both the active and passive signatures are functions of geometric and dielectric properties of soil, an integrated AP modeling approach may yield more biophysically realistic updates of the model states and parameters. Such an integrated approach also ensures robustness when assimilating both asynchronous (e.g., SMOS and ALOS-PALSAR) and synchronous (e.g., SMAP) AP observations, in operational use. Integrated AP models have been developed and tested for bare soil, such as the integral equation method (IEM) [23], [24]. The IEM model [25], [26], which is based on the Kirchoff approximation, represents the rough surface as tangential surface slopes and estimates the scattered field as the summation of two components given by the Kirchoff and complementary scattered fields. The emissivity, which is used to estimate T_B, is calculated by integrating the bistatic scattering coefficients.

Ensemble-based assimilation techniques such as the ensemble Kalman filter (EnKF) have been widely used for land data assimilation research and applications since they can be applied to nonlinear and discontinuous models [27], such as the SVAT and IEM models. Reichle *et al.* [3], [4] applied the EnKF and the extended Kalman filter (EKF) to assimilate T_B observations and estimate SM profile, showing an error lower than 2.0% SM in the estimates. The EnKF provided results closer to the observations than the EKF for applications with nonlinear functions. Since then, it has emerged as the algorithm of choice for SM data assimilation in many studies [2]–[4], [9], [28]–[32]. However, the EnKF algorithm minimizes only the random errors and assumes that the system is unbiased. Reichle and Koster [33] compared three independent surface SM data sets and found large discrepancies, demonstrating the need for bias estimation and correction in assimilation frameworks to estimate SM. Because of the difficulty in characterizing the bias in observations, they are often assumed to be unbiased [34].

Bias correction methods range from simple algorithms [35] to more complex correction frameworks that estimate and correct bias in EnKF-based assimilation algorithms [36]. Some studies utilize the augmented state vector (e.g., [28] and [31]) and update the states and model parameters simultaneously to correct bias. However, the EnKF may become unstable when a large number of parameters are included in the state vector. In such cases, an integrated bias value could be estimated to correct the model estimates. Friedland [37] demonstrated that the Kalman filter equations for the augmented state are algebraically equivalent to two coupled recursive filters, resulting in a two-stage estimation algorithm. The first stage consists of the standard Kalman filter obtained by ignoring the bias (bias-blind filter) [37]–[39]. The second stage provides estimates of the bias based on the output of the first stage. Dee and Da Silva [38] presented how to estimate the bias sequentially in a data-assimilation system and its online implementation for unbiased observations. Considering that the time-mean prior error is approximately constant in time, the bias correction algorithms use a persistent bias model during the propagation phase, i.e., it is constant between two consecutive observations. DeLannoy *et al.* [36] conducted an implementation of Friedland's algorithm using the EnKF in a synthetic study to assimilate SM observations. In this method, the initial value for the bias was assumed zero, and the bias covariance was calculated using the empirical γ factor relating the bias covariance to the state covariance [38], [39]. The results were found to be sensitive to the initial value of the bias. In addition, the empirical factor used in the model could overestimate the bias to compensate for other errors in modeled states. However, a major gap exists in using any of the current bias estimation methods for nonlinear observation operators such as those relating T_B and σ^0 to SM. In this paper, the methodology presented in Dee and Da Silva [38] will be extended to nonlinear observation operator such as the AP model and estimate the bias covariance without prior information.

The goal of this study is to implement a bias correction methodology that incorporates a nonlinear observation operator in two different approaches to understand their impact on SM estimates from assimilation of AP observations at L-band. In this paper, we implement an EnKF-based algorithm and two bias correction approaches with a nonlinear observation operator, viz., a simultaneous state parameter (SSP) update and an online estimation and correction of bias with feedback (BCWF), to assimilate AP observations directly in an SVAT model linked with an integrated AP model. We use both synthetic and field observations from the Eleventh Microwave Water Energy Balance Experiment (MicroWEX-11) to analyze the impact of assimilating AP observations on SM estimates under bare soil conditions. The objectives of this study are as follows: 1) to develop a bias correction framework for nonlinear observation operators; 2) to implement the framework within an assimilation algorithm using AP observations; and 3) to evaluate the two bias correction approaches for their impact on SM estimates when assimilating synthetic and field microwave observations. The assimilation using the field observations provides insights into the model physics, unlike synthetic studies in which the observations are typically obtained from the same model or models using similar physics. The methodology developed here can be extended to studies under different terrain conditions for various hydroclimatic regions.

In the next sections, we briefly describe the MicroWEX-11 observations, the linked SVAT-AP model, and the EnKF framework used in this study to correct model bias.

II. MicroWEX-11

MicroWEX-11 was conducted in 2012 on a 9.6-acre field from day of the year (DoY) 129 (May 8) to DoY 165 (June 13) in North Central Florida. The objective of the experiment was to observe microwave signatures of bare soil over smooth conditions. The soils at the site were lake fine sand, with 89.4% sand, 7.1% clay, and a bulk density of 1.55 g/cm^3. Data used in this study include microwave brightness temperatures, backscattering coefficients, SM, wind speed, upwelling and downwelling short- and longwave radiation, precipitation, irrigation, relative humidity, and air temperature measured every 15 min. Horizontally polarized microwave brightness temperatures were measured by the tower-mounted University of Florida L-band Microwave Radiometer (UFLMR), operating at the center frequency of 1.4 GHz and observing a footprint of 4.29 m X 7.08 m from a height of 6.81 m. The active observations

were conducted using the University of Florida L-band Automated Radar System (UFLARS) at 1.25 GHz providing σ^0 in four polarization combinations (HH, VV, HV, and VH). The SM values were observed at 2, 4, 8, 16, and 64 cm, using Campbell Scientific Water Content Reflectometers. Four tipping-bucket rain gauges logged precipitation and irrigation at the field site.

III. LSP-AP Model

The SVAT model used in this study is the land surface process (LSP) model [1], [40]. The LSP model was linked with the integrated AP model to provide the T_B and σ^0 estimates at both vertical (V) and horizontal (H) polarizations (pols). In the LSP-AP model, the LSP model provides the AP model with estimates of soil moisture and temperature profiles. Such linked models can be used to estimate the microwave signatures without the need of *in situ* observations of SM and soil temperature observations.

A. LSP Model

The LSP model simulates 1-D coupled energy and moisture transport in soil and vegetation using diffusion-type equations and estimates energy and moisture fluxes at the land surface and in the root zone. The model is forced with micrometeorological parameters such as air temperature, relative humidity, downwelling solar and longwave radiation, irrigation/precipitation, and wind speed. The LSP model includes 16 parameters [28], with four parameters related to radiation balance, eight to latent and sensible heat fluxes, and the remaining four to the soil hydraulic properties. The sensible heat flux is calculated using the bulk transfer approach from [41] and the latent heat flux following [42]. The soil energy balance is calculated following the equations from [43] and [44].

The number of soil layers, with uniform constitutive properties, is user defined. Two layers are used for this study: the first layer, the top 1.7 m of soil, is primarily sandy, with 89.4% sand, and the second layer (1.7–2.7 m) constituted 40.5% sand. The soil has 35 computational blocks (nodes) in the two layers. The thickness of the blocks increases exponentially, with four blocks in the top 5 cm of the soil, appropriate for capturing the highly dynamic moisture transport near the soil surface. A block-centered finite-differential scheme is employed to solve the coupled governing equations and estimate energy and moisture fluxes at land surface and in the root zone at an adaptive time step (seconds/minutes) in response to the forcings [45].

B. Integrated AP Model

A compact expression of IEM to compute the bistatic scattering coefficient is [24]

$$\sigma^0_{\mathrm{soil},qp}(\theta_i,\phi_i;\theta_s,\phi_s) = \frac{k_i^2}{2}\exp\left[-\sigma^2\left(k_{iz}^2+k_{sz}^2\right)\right] \times \sum_{n=1}^{\infty}\frac{\sigma^{2n}}{n!}\left|I^n_{qp}\right|^2 W^{(n)}(k_{sx}-k_{ix},k_{sy}-k_{iy}) \quad (1)$$

where

$$\hat{k_i} = k_{ix}\hat{x}+k_{iy}\hat{y}+k_{iz}\hat{z} = k_i\sin\theta_i\cos\phi_i\hat{x}+k_i\sin\theta_i\sin\phi_i\hat{y}+k_i\cos\theta_i\hat{z} \quad (2a)$$

$$\hat{k_s} = k_{sx}\hat{x}+k_{sy}\hat{y}+k_{sz}\hat{z} = k_s\sin\theta_s\cos\phi_s\hat{x}+k_s\sin\theta_s\sin\phi_s\hat{y}+k_s\cos\theta_s\hat{z} \quad (2b)$$

where k is the wavenumber, σ^2 is the variance of the surface heights, and $W^{(n)}(k_{sx}-k_{ix},k_{sy}-k_{iy})$ is the roughness spectrum of the surface related to the nth power of the surface correlation function. The analytical expressions to compute I^n_{qp} are given in [24].

The surface emissivity is related to the bistatic scattering coefficient by

$$e_p(\theta_i,\phi_i) = 1-\frac{1}{4\pi}\int_0^{2\pi}\int_0^{\frac{\pi}{2}}\left[\sigma^0_{\mathrm{soil},pp}(\theta_i,\phi_i;\theta_s,\phi_s) + \sigma^0_{\mathrm{soil},qp}(\theta_i,\phi_i;\theta_s,\phi_s)\right]\frac{\sin\theta_s}{\cos\theta_i}d\theta_s d\phi_s \quad (3)$$

where $\sigma^0_{\mathrm{soil},pq}$ is the bistatic coefficient at pq polarization; and (θ_i,ϕ_i) and (θ_s,ϕ_s) are the incident and scattering directions, respectively.

In the case of a bare soil, T_B is given by [46]

$$T_{B,p} = T_{\mathrm{eff}}e_p + T_{\mathrm{Bsky}}(1-e_p) \quad (4)$$

where $p=\{v,h\}$ is the sensor polarization, e is the surface emissivity, T_{eff} is the effective temperature of the soil, and T_{Bsky} is the brightness temperature of sky. At low frequencies, such as at L-band, T_{Bsky} is low, ranging between 2 and 4 K.

IV. Bias Correction With Nonlinear Operators

In this paper, an EnKF-based assimilation algorithm was used to correct bias when assimilating passive-only, active-only, and both AP microwave observations and using the LSP-AP model. Most of the current studies that correct bias within an EnKF framework are based on the assumption that variables of the state vector and observations belong to the same space [4], [28], [33]. However, when assimilating microwave observations for improving SM estimates, the variables of the state vector and observations are not in the same space. Moreover, the AP observations are nonlinearly related to SM. It is necessary to use a nonlinear observation operator, such as a microwave model, that links the state vector to the observations. This section presents the derivation of the update and analysis equations for the two different stages presented in [37] and [38] in the case of a nonlinear observation operator.

A. EnKF for Nonlinear Observation Operators

The state equation for each realization [47] is given by

$$x_t^{i-} = f\left(x_{t-1}^{i+},u_{t-1}^i,\theta_{t-1}^+\right)+\eta_{t-1}^i \quad (5)$$

where $f(\cdot)$ is the nonlinear model, x_t^{i-} is the state of the ith ensemble prior to the update at time t, x_{t-1}^{i+} is the posterior state of the ith ensemble at time $t-1$, u_{t-1}^i represents the meteorological forcing data for the ith ensemble member, θ_{t-1}^+ represents the model parameters, and η_{t-1}^i is the model error. In our study, the model physics are assumed to be perfect ($\eta_{t-1}^i = 0$).

The nonlinear observation operator $\mathcal{M}$ relates x_t^{i-} to the observations, i.e.,

$$d_t^i = \mathcal{M}\left(x_t^{i-}\right) + \epsilon_t^i \tag{6}$$

where ϵ_t^i is the error in the observations and is generally assumed Gaussian with zero mean and variance R_e.

The ensemble of state vectors x_t^i and the perturbed observations d_t^i can be represented in a matrix form as

$$A_t = \left\{x_t^1, x_t^2, \cdots, x_t^N\right\} \tag{7}$$

$$D_t = \left\{d_t^1, d_t^2, \cdots, d_t^N\right\} \tag{8}$$

where N is the number of ensembles.

The posterior matrix of state vectors A_t^+ is computed as a linear combination of the prior estimate A_t^- and the observation matrix D_t weighted by the Kalman gain [22], [48], i.e.,

$$A_t^+ = A_t^- + A_t'\mathcal{M}\left(A_t'\right)^T \times \left(\mathcal{M}\left(A_t'\right)\left(\mathcal{M}(A_t')\right)^T + \gamma\gamma^T\right)^{-1} \times \left(D_t - \mathcal{M}\left(A_t^-\right)\right) \tag{9}$$

where $A_t' = A_t^- - \bar{A}_t$, $\bar{A}_t$ is the means of A_t^-, and γ is the ensemble of observation errors. The variance in the observation error is assumed to be $R_e = (1/(N-1))\gamma\gamma^T$.

B. Online Bias Correction Approach for Nonlinear Observation Operators

The biased state equation can be represented as [47]

$$x_t^{i-} = f\left(x_{t-1}^{i+}, u_{t-1}^i, \theta_{t-1}^+\right) \tag{10}$$

where $f(\cdot)$ is the nonlinear model, x_t^{i-} is the state of the ith ensemble member prior to the update at time t, x_{t-1}^{i+} is the posterior state of the ith ensemble member at time $t-1$, u_{t-1}^i represents the meteorological forcing for the ith ensemble member, and θ_{t-1}^+ represents the model parameters.

The prior bias b_t^{i-} at time t is defined as the expectation of the prior error, which is given by the true state x_t^{true} and the biased prior state x_t^{i-}. This is

$$b_t^{i-} = E\left\{x_t^{\text{true}} - x_t^{i-}\right\}. \tag{11}$$

In general, the prior bias can be time dependent, but for the purposes of this study, we consider a constant bias model to propagate the bias estimate in time between consecutive assimilation updates [38], i.e.,

$$\hat{b}_t^{i-} = \hat{b}_{t-1}^{i+}. \tag{12}$$

Considering that the bias is only due to the model and if the prior bias were known, the unbiased prior state can be computed by

$$\tilde{x}_t^{i-} = x_t^{i-} - \hat{b}_t^{i-}. \tag{13}$$

The nonlinear operator $\mathcal{M}$ relates x_t^{i-} to the observations, i.e.,

$$d_t^i = \mathcal{M}\left(x_t^{i-}\right) + \epsilon_t^i \tag{14}$$

where ϵ_t^i is the error in the observations and is generally assumed Gaussian with zero mean and variance R_e.

The bias-blind analysis equation is

$$x_t^{i+} = x_t^{i-} + K_t\left[d_t^i - \mathcal{M}\left(x_t^{i-}\right)\right] \tag{15}$$

with

$$K_t = \tilde{S}_{xd}[\tilde{S}_{dd} + R_e]^{-1} \tag{16}$$

where $\tilde{S}_{xd}$ is the cross covariance between the prior unbiased state and its transformation value in the observation space, and $\tilde{S}_{dd}$ is the covariance of the transformed prior unbiased states in observation space.

The posterior bias estimate $\hat{b}_t^{i+}$ is obtained as a linear combination of the prior bias estimate $\hat{b}_t^{i-}$ and the difference between the observations and the prior bias-corrected state estimate [37], [38], i.e.,

$$\begin{aligned}\hat{b}_t^{i+} &= \hat{b}_t^{i-} - L_t\left[d_t^i - \mathcal{M}\left(\tilde{x}_t^{i-}\right)\right] \\ &= \hat{b}_t^{i-} - L_t\left[d_t^i - \mathcal{M}\left(x_t^{i-} - \hat{b}_t^{i-}\right)\right].\end{aligned} \tag{17}$$

If the $\mathcal{M}$ operator is a continuous derivative function at time t, we can define the linearized observation operator [38]

$$N_t \equiv \frac{\partial \mathcal{M}}{\partial x}\Big|_{x=x_t^{i-}}. \tag{18}$$

Equation (17) can be rewritten as

$$\hat{b}_t^{i+} = \hat{b}_t^{i-} - L_t\left[d_t^i - \mathcal{M}\left(x_t^{i-}\right) - N_t\hat{b}_t^{i-}\right] \tag{19}$$

with

$$L_t = S_{b,t}^- N_t^T\left[N_t S_{b,t}^- N_t^T + \tilde{S}_{dd} + R_e\right]^{-1} \tag{20}$$

where $S_{b,t}^-$ is the prior bias error covariance.

C. Bias Estimation for Nonlinear Observation Operators to the EnKF

This section presents the extension of the equations derived earlier for the EnKF based on [38] and [48]. In the EnKF, the cross covariance and the covariance in the Kalman gains, i.e., K_t and L_t, can be calculated from the ensemble statistics.

The ensemble of state vectors x_t^i, the ensemble of the bias vectors $\hat{b}_t^i$, and the perturbed observations d_t^i can be represented

in a matrix form, respectively, as

$$A_t = \left\{x_t^1, x_t^2, \cdots, x_t^N\right\} \tag{21}$$

$$\hat{B}_t = \left\{\hat{b}_t^1, \hat{b}_t^2, \cdots, \hat{b}_t^N\right\} \tag{22}$$

$$D_t = \left\{d_t^1, d_t^2, \cdots, d_t^N\right\} \tag{23}$$

where N is the number of ensembles.

The bias-blind analysis equation becomes

$$A_t^+ = A_t^- + \tilde{S}_{xd}[\tilde{S}_{dd} + R_e]^{-1}\left[D_t - \mathcal{M}\left(A_t^-\right)\right]. \tag{24}$$

Defining the ensemble perturbation matrix of the unbiased state vector as $\tilde{A}_t' = \tilde{A}_t^- - \bar{\tilde{A}}_t$, with $\bar{\tilde{A}}_t$ being the mean matrix of $\tilde{A}_t^-$, and the ensemble perturbation matrix of the prior unbiased states in the observation space as $\mathcal{M}'(\tilde{A}_t) = \mathcal{M}(\tilde{A}_t^-) - \bar{\mathcal{M}}(\tilde{A})$, with $\bar{\mathcal{M}}(\tilde{A})$ being the mean matrix of $\mathcal{M}(\tilde{A}_t^-)$, $\tilde{S}_{xd}$ and $\tilde{S}_{dd}$ can be calculated by [22], [48]

$$\tilde{S}_{xd} = \frac{\tilde{A}_t'\mathcal{M}'(\tilde{A}_t)^T}{N-1} \tag{25}$$

$$\tilde{S}_{dd} = \frac{\mathcal{M}'(\tilde{A}_t)\mathcal{M}'(\tilde{A}_t)^T}{N-1} \tag{26}$$

where $\tilde{A}_t'$ is the ensemble perturbation matrix for the unbiased state vector.

Equation (24) can be rewritten as

$$A_t^+ = A_t^- + \tilde{A}_t'\mathcal{M}'(\tilde{A}_t)^T \times \left[\mathcal{M}'(\tilde{A}_t)\mathcal{M}'(\tilde{A}_t)^T + R_e\right]^{-1} \times \left[D_t - \mathcal{M}\left(A_t^-\right)\right]. \tag{27}$$

The posterior bias estimates for the EnKF are given by

$$\hat{B}_t^+ = \hat{B}_t^- - L_t\left[D_t - \mathcal{M}\left(A_t^-\right) - N_t\hat{B}_t^-\right]. \tag{28}$$

Similar to (25) and (26), the Kalman gain L_t can be calculated using the statistics of the ensembles as

$$L_t = \hat{B}_t'\left(N_t\hat{B}_t'\right)^T\left[N_t\hat{B}_t'\hat{B}_t'^T N_t^T + \mathcal{M}'(\tilde{A}_t)\mathcal{M}'(\tilde{A}_t)^T + R_e\right]^{-1} \tag{29}$$

where $\hat{B}_t'$ is the ensemble perturbation of the bias vector defined as $\hat{B}_t' = \hat{B}_t^- - \bar{\hat{B}}_t$, with $\bar{\hat{B}}_t$ being the mean matrix of $\hat{B}_t^-$.

V. Analysis Equations for the EnKF-Based Bias Correction Approaches

A. Bias Correction Method With Feedback (BCWF)

The estimation of unbiased states requires the prediction of the prior state vector and the prior bias vector, the solution of the bias update equations, and the solution of the analysis equation. As mentioned in [38], a more efficient algorithm is the one that uses the prior bias estimates as soon as they are available in order to generate unbiased estimates. This procedure introduces feedback information from the updated bias estimates to the original system. This section presents the solution of the bias update equation and the solution of the analysis equation for the BCWF method.

1) The prior state vector and the prior bias vector are given by

$$x_t^{i-} = f\left(\tilde{x}_{t-1}^{i+}, u_{t-1}^i, \theta_{t-1}^+\right) \tag{30}$$

$$d_t^i = \mathcal{M}\left(\tilde{x}_t^{i-}\right) + \epsilon_t^i \tag{31}$$

$$\hat{b}_t^{i-} = \hat{b}_{t-1}^{i+} \tag{32}$$

$$\tilde{x}_t^{i-} = x_t^{i-} - \hat{b}_t^{i-}. \tag{33}$$

2) The bias update equation in the EnKF framework is

$$\hat{B}_t^+ = \hat{B}_t^- - L_t\left[D_t - \mathcal{M}\left(A_t^-\right) - N_t\hat{B}_t^-\right] \tag{34}$$

$$L_t = \hat{B}_t'\left(N_t\hat{B}_t'\right)^T\left[N_t\hat{B}_t'\hat{B}_t'^T N_t^T + \mathcal{M}'(\tilde{A}_t)\mathcal{M}'(\tilde{A}_t)^T + R_e\right]^{-1} \tag{35}$$

$$\tilde{A}_t^+ = A_t^+ - \hat{B}_t^+. \tag{36}$$

3) The analysis equations are

$$\tilde{\tilde{A}}_t^+ = \tilde{A}_t^- + K_t\left[D_t - \mathcal{M}\left(\tilde{A}_t^-\right)\right] \tag{37}$$

$$K_t = \tilde{A}_t'\mathcal{M}'(\tilde{A}_t)^T\left[\mathcal{M}'(\tilde{A}_t)\mathcal{M}'(\tilde{A}_t)^T + R_e\right]^{-1}. \tag{38}$$

B. SSP Update

In this approach, an augmented state vector is used, which includes the parameters to which the states are most sensitive, along with the states to be updated in the filter. Thus, the augmented state vector is

$$A_{\mathrm{SSP},t} = \begin{bmatrix} x_t^1, x_t^2, \cdots, x_t^N \\ \Theta_t^1, \Theta_t^2, \cdots, \Theta_t^N \end{bmatrix} \tag{39}$$

where $\{x_t^1, x_t^2, \cdots, x_t^N\}$ represents the ensemble of states, and $\{\Theta_t^1, \Theta_t^2, \cdots, \Theta_t^N\}$ represents the ensemble of sensitive model parameters. Equation (9) is also applicable for this technique. In this approach, the bias is assumed that the improved parameter estimation results in reduction or elimination of the bias.

VI. Methodology

A. LSP-AP Simulations

Model simulations using the LSP-AP model were conducted for smooth bare soil conditions for 15 days, from DoY 129 to DoY 144 in 2012 during MicroWEX-11. Micrometeorological forcings for the simulations were obtained from MicroWEX-11. Initial moisture and temperature conditions were obtained from the first values observed by the SM and temperature sensors on DoY 129. The values of the 16 parameters of the LSP model are shown in Table I obtained from [19]

TABLE I
PARAMETERS INCLUDED IN THE LSP MODEL [45]. THE VALUES FOR CANOPY PARAMETERS WERE FROM [54], AND RANGES FOR SOIL PARAMETERS WERE FROM [55]. THE RANGES OF PARAMETERS CONSIDERED AS SOURCE OF UNCERTAINTY IN THE LSP AND AP MODELS WERE OBTAINED FROM [19] AND [28]

Model		Parameter	Description	Values
LSP	CANOPY	z_{ob}	Bare soil roughness length (m)	0.004
		x	Leaf angle distribution parameter	0.819
		σ	Leaf reflectance	0.474
		ϵ_c	Canopy emissivity	0.973
		ϵ_s	Soil emissivity	0.953
		c_d	Canopy drag coefficient	0.328
		i_w	Canopy wind intensity factor	67.9
		l_w	Leaf width (m)	0.0531
		F_b	Base assimilation rate (kg CO_2/m^{2}s)	$-0.82X10^{-8}$
		ϵ_{photo}	Photosynthetic efficiency (kg CO_2/J)	$0.897X10^{-6}$
		$soil_a$	Slope parameter for r_s (m^{2}s/kg H_2O)	370
		$soil_b$	Intercept parameter for r_s (m^{2}s/kg H_2O)	-531
	SOIL (0-1.7 m)	λ	Pore-size index	$0.1 - 0.9$
		ψ_0	Air entry pressure (m H_2O)	$0.05 - 1.0$
		K_{sat}	Saturated hydraulic conductivity (m/s)	$10^{-5} - 10^{-3}$
		ϕ	Porosity (m^3/m^3)	$0.2 - 0.55$
	SOIL (1.7-2.7 m)	λ	Pore-size index	0.05
		ψ_0	Air entry pressure (m H_2O)	0.019
		K_{sat}	Saturated hydraulic conductivity (m/s)	$8.93X10^{-5}$
		ϕ	Porosity (m^3/m^3)	0.41
AP	SOIL (surface)	h_{rms}	Surface RMS height (m)	$0 - 0.05$
		cl	Surface correlation length (m)	$0 - 0.50$

and [28]. The SM and temperature values provided by the LSP model were used to calculate the soil dielectric constant using [49], and the soil dielectric properties were given to the AP model. The microwave observations are simulated at 1.26 GHz for active, matching those of the SMAP, and at 1.42 GHz for passive, matching the SMOS and SMAP observations. The incidence angle was set to 40°, matching the UFLMR and UFLARS observations during MicroWEX-11. The correlation function of the rough surface is assumed to be exponential based on field observations during MicroWEX-11. The RMS height and correlation length were 0.69 and 9.57 cm, respectively, based on field observations [50].

B. Implementation of the EnKF

In this paper, the nonlinear propagator $f(\cdot)$ in (5) represents the LSP model, x is the state vector consisting of near-surface SM and root-zone SM (RZSM) estimates by the LSP model, and the $\mathcal{M}$ operator represents the AP model transforming SM into $T_{B,v}$, $T_{B,h}$, σ^0_{vv}, and σ^0_{hh}; u_t is the vector of meteorological forcings at time t, and θ are the model parameters of the LSP model. The ith ensemble at time t is therefore expressed as

$$x_t^i = \begin{bmatrix} \text{SM}_t^i \\ \text{RZSM}_t^i \end{bmatrix}. \tag{40}$$

The SM and RZSM estimates and observations were calculated by the equation

$$\text{SM or RZSM} = \sum_{i=1}^{k} \text{SM}_i \Delta z_i \tag{41}$$

where k indicates the total number of blocks within 0–5 cm or the root zone in the LSP model, Δz_i indicates the thickness of the ith block, and SM_i indicates the volumetric SM in the ith block. The thickness for each block is presented in Table III. The contribution provided by each block to the RZSM estimates is given by the ratio

$$r_i = \frac{\Delta z_i \text{SM}_i}{\text{RZSM}}. \tag{42}$$

The states at the observation space are

$$\mathcal{M}\left(x_t^i\right) = \begin{bmatrix} T_{B,v,t}^{i\ *} \\ T_{B,h,t}^{i\ *} \\ \sigma_{vv,t}^{0,i\ **} \\ \sigma_{hh,t}^{0,i\ **} \\ \text{SM}^{***} \end{bmatrix}$$

*included in the vector when passive observations are available

**included in the vector when active observations are available

***included in the vector when assimilating SM observations. (43)

Two hundred $(N = 200)$ ensembles realizations were used for assimilation to achieve reliable estimates [21], [28]. The sources of uncertainty were the soil parameters in the LSP model and the forcing data. The open-loop simulations of the model were conducted using the 16 parameters, with four uncertain parameters, viz., ϕ, λ, K_{sat}, and ψ_0, that were uniformly distributed within the literature-based ranges, as shown in Table I [28]. Among all the inputs/forcings to the LSP model, precipitation/irrigation observations typically have the highest errors compared with other micrometeorological parameters. A Gaussian error with zero mean and standard deviation equal to 12% of the observed precipitation/irrigation value was introduced during events [51], [52]. An error with a Poisson distribution and 0.45 mean was introduced in the absence of the

TABLE II
SOURCES OF UNCERTAINTY IN FORCING VARIABLES [9]

Forcing variable	Distribution	Parameter
Air temperature	Additive Gaussian	μ=0, σ=3K
Shortwave radiation	Multiplicative Gaussian	μ=0, σ=0.1
Relative humidity	Additive Gaussian	μ=0, σ=1.0%
Wind speed	Additive Gaussian	μ=0, σ=0.3 ms^{-1}
Precipitation event	Multiplicative Gaussian	μ=0, σ=12%
No-precipitation event	Poisson	μ=0.45

events. In this paper, forcing variables vary within a physically reasonable range based on [9], as shown in Table II.

For the synthetic study, the bias was introduced by a constant function of 0.0015 m^3/m^3 in the SM estimates, for every ensemble member in the EnKF, provided by the LSP model at each step. The bias remained unchanged during the propagation phase.

C. Implementation of Bias Correction Algorithms

1) SSP: In the bias correction through update of the sensitive parameters, the augmented state vector is composed of the SM and RZSM estimates and the parameters porosity (ϕ) and pore-size index (λ) from the LSP model (Table III presents the node thickness to calculate the SM and RZSM observation). The selection of the sensitive parameters was based on the results of [21] and [28]. The augmented state vector is therefore

$$x^i_{\mathrm{SSP},t} = \begin{bmatrix} \mathrm{SM}^i_t \\ \mathrm{RZSM}^i_t \\ \phi^i_t \\ \lambda^i_t \end{bmatrix}. \tag{44}$$

The vector representing the state at the observations space remains the same as (43).

2) Online Bias Correction: In the BCWF method, the state vector x^i_t and the observation vector $\mathcal{M}(x^i_t)$ are similar to (40) and (43), and the bias state vector b^{i-}_t is defined as

$$b^{i-}_t = \begin{bmatrix} b^{i-}_{\mathrm{SM},t} \\ b^{i-}_{\mathrm{RZSM},t} \end{bmatrix}. \tag{45}$$

The initial bias in the BCWF method was a Gaussian function with zero mean and standard deviation of 4% of SM.

D. Synthetic and Field Observations

The synthetic truth was obtained from one of the realizations from an unbiased open-loop simulation of the LSP-AP model. The truth was not included in the ensemble of 200 members during the assimilation. The field observations were obtained from the MicroWEX-11 experiment, described in Section II. A Gaussian error with zero mean and standard deviation of 4 K was added to brightness observations, and a Gaussian error with zero mean and standard deviation of 1 dB was added to active observations based on field observations. For SM observations, the truth was perturbed with a Gaussian error with zero mean and 0.02 m^3/m^3 standard deviation.

E. Assimilation Experiments

Different assimilation scenarios with synthetic observations of T_B and σ^0 were performed. The performances of the bias correction methods presented in Section IV were compared by assimilating H pol for passive and VV pol for active observations due to the high sensitivity of these polarizations to detect variations in SM. The performance of the bias correction methods was used to understand the improvements in the SM estimates from assimilation scenarios involving passive-only, active-only, and active/passive observations. The assimilation experiment using *in situ* observations of $T_{B,h}$ and σ^0_{vv} from MicroWEX-11 is conducted using the two bias correction methods. The temporal frequency of assimilation for both the synthetic and field observations is every three days at 6 A.M. EST, corresponding to the availability of current and near-future remotely sensed microwave observations [6], [7]. The SM represented near-surface SM (0–5 cm), comparable with that derived from remote sensing measurements, and the integrated SM at 0–100 cm represented the RZSM.

VII. RESULTS AND DISCUSSION

A. Assimilation of Synthetic Observations

1) Assimilation of SM Observations: The two bias correction methods, namely, SSP and BCWF, were compared in terms of the time average standard deviation (ASD) in the SM estimates of the ensemble, the time root-mean-square error (RMSE) between the estimates and their respective true values, and the time average bias (AB). The AB was estimated by applying (11). In general, lower ASDs imply higher certainty in the estimates, and lower RMSEs imply better accuracy. Table IV summarizes these values when assimilating SM synthetic observations. The SM estimates improved in comparison with open-loop simulations when the standard EnKF was applied. When the bias correction methods were applied, the SM estimates improved by 31% (SSP) and 39% (BCWF) compared with open-loop simulations and by 8% (SSP) and 19% (BCWF) compared with the EnKF. In all cases, the AB from the two bias correction methods reduced compared with the open loop and the EnKF. This indicates the need to implement bias correction methods to improve the SM estimates.

Between the two bias correction methods, the BCWF resulted in the lowest RMSE and the lowest ASD for the SM estimates. While the BCWF compensates the bias by correcting the posterior state estimates with the posterior bias estimates using (30)–(38), the SSP compensates for the bias by modifying the parameter values of the ensemble. Unlike real field observations where the bias may be, primarily, from the parameters, in this study, the bias effects were represented by introducing a constant value at every step in SM. The low performance of the SSP compared with the BCWF is because the parameters are not the source of bias in this case.

Fig. 1(a) shows the time series of the ensemble mean of the SM estimates. Throughout the simulation period, the open-loop simulations present the highest difference in comparison with the truth. When comparing the simulations of the two bias correction methods and the EnKF simulations, it is observed

TABLE III
NODE THICKNESS USED TO CALCULATE THE SM AND RZSM OBSERVATIONS IN (41)

LSP model						Observations	
Depth (cm)	Δz_i (cm)	Depth (cm)	Δz_i (cm)	Depth (cm)	Δz_i (cm)	Depth (cm)	Δz_i (cm)
0.5	1.50	17.23	2.75	60.64	7.01	$0-5$	2.92
1.55	1.17	19.96	3.00	67.70	7.76	8	3.00
2.71	1.25	22.95	3.25	75.47	8.59	16	6.01
3.98	1.42	26.25	3.67	84.02	9.42	32	28.02
5.37	1.50	29.87	3.92	93.42	6.59	64	52.04
6.91	1.75	33.86	4.42			120	8.01
8.60	1.83	38.25	4.84				
10.46	2.00	43.07	5.34				
12.51	2.25	48.38	5.84				
14.76	2.50	54.22	6.42				

TABLE IV
ROOT-MEAN-SQUARE ERROR (RMSE) BETWEEN THE TRUTH AND THE ESTIMATES OF NEAR-SURFACE SOIL MOISTURE (SM), RZSM, $T_{B,h}$, σ^0_{vv}, THEIR TIME AVERAGE BIAS (AB), AND THEIR ASSOCIATED AVERAGE STANDARD DEVIATION (ASD) WHEN USING BIAS CORRECTION METHODS AND ASSIMILATING MICROWAVE SYNTHETIC OBSERVATIONS. THE BIAS CORRECTION METHODS ARE THE SIMULTANEOUS STATE PARAMETER (SSP) UPDATE AND THE BIAS CORRECTION WITH FEEDBACK (BCWF) UPDATE

Scenario	Method	SM			$RZSM$			$T_{B,h}$		σ^0_{vv}	
		$RMSE$ $(vol\%)$	AB $(vol\%)$	ASD $(vol\%)$	$RMSE$ $(vol\%)$	AB $(vol\%)$	ASD $(vol\%)$	$RMSE$ (K)	ASD (K)	$RMSE$ (dB)	ASD (dB)
Open-loop		9.70	9.54	4.72	8.99	8.78	3.75	35.22	12.43	4.75	-24.83
SM	EnKF	7.27	7.14	2.98	5.26	5.09	1.42	—-	—-	—-	—-
	SSP	6.77	6.55	3.79	4.72	4.53	1.56	—-	—-	—-	—-
	BCWF	5.96	5.79	3.31	3.18	3.05	2.16	—-	—-	—-	—-
$T_{B,h}$	EnKF	7.39	7.27	2.98	5.42	5.29	1.52	28.94	7.83	—-	—-
	SSP	6.66	6.49	3.66	4.84	4.68	1.48	26.16	9.42	—-	—-
	BCWF	5.50	5.33	2.99	2.82	2.56	1.85	23.47	7.86	—-	—-
σ^0_{vv}	EnKF	7.38	7.26	3.27	5.48	5.35	1.57	—-	—-	4.06	-26.71
	SSP	6.50	6.29	2.28	5.56	5.39	1.45	—-	—-	3.59	-28.36
	BCWF	5.20	4.96	2.59	2.42	2.16	1.55	—-	—-	3.30	-27.87
$T_{B,h}$+σ^0_{vv}	EnKF	7.29	7.16	3.05	5.28	5.12	1.42	28.70	8.05	4.02	-27.05
	SSP	6.70	6.45	1.22	5.59	5.22	0.91	26.85	3.52	3.75	-30.17
	BCWF	5.54	5.36	2.71	3.07	2.89	2.12	23.60	7.39	3.47	-27.90

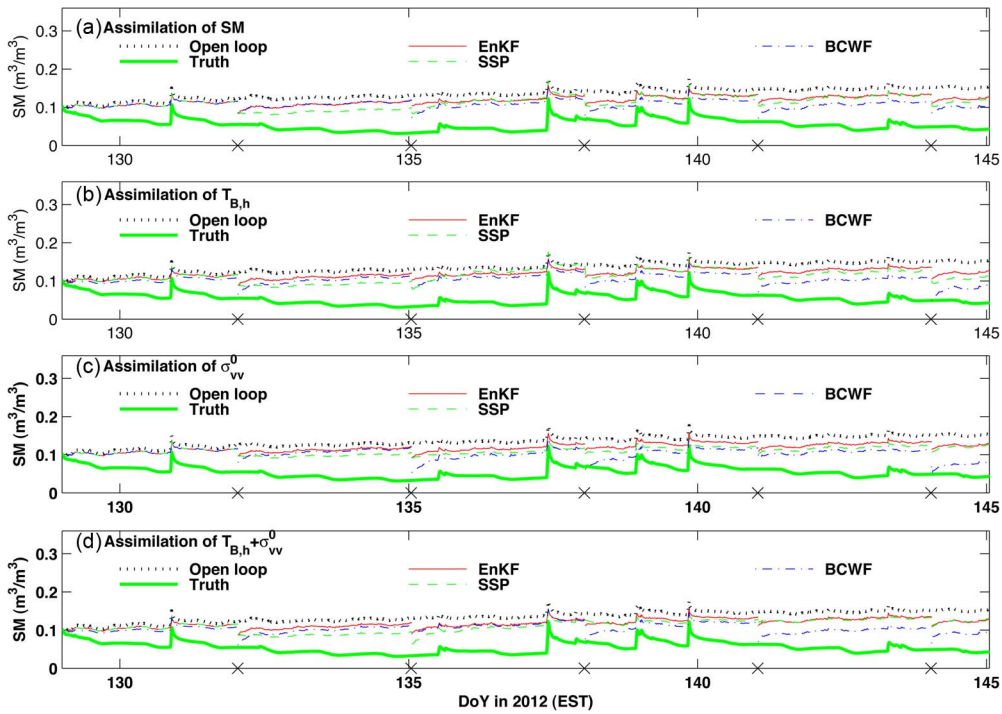

Fig. 1. Estimates of SM when assimilating synthetic observations of (a) SM, (b) $T_{B,h}$ (c) σ^0_{vv}, and (d) $T_{B,h}+\sigma^0_{vv}$ when using the EnKF and the bias correction methods: SSP and BCWF.

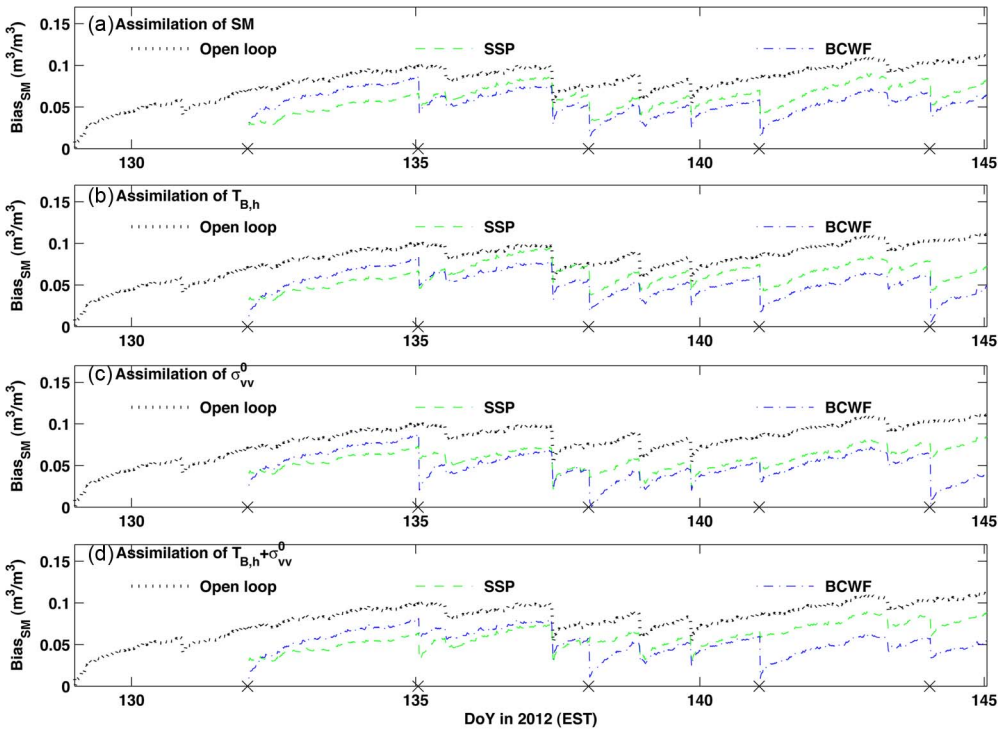

Fig. 2. (a)–(d) Estimates of bias in SM when assimilating synthetic observations of SM, passive, active, and AP and using the EnKF and the bias correction methods: SSP and BCWF.

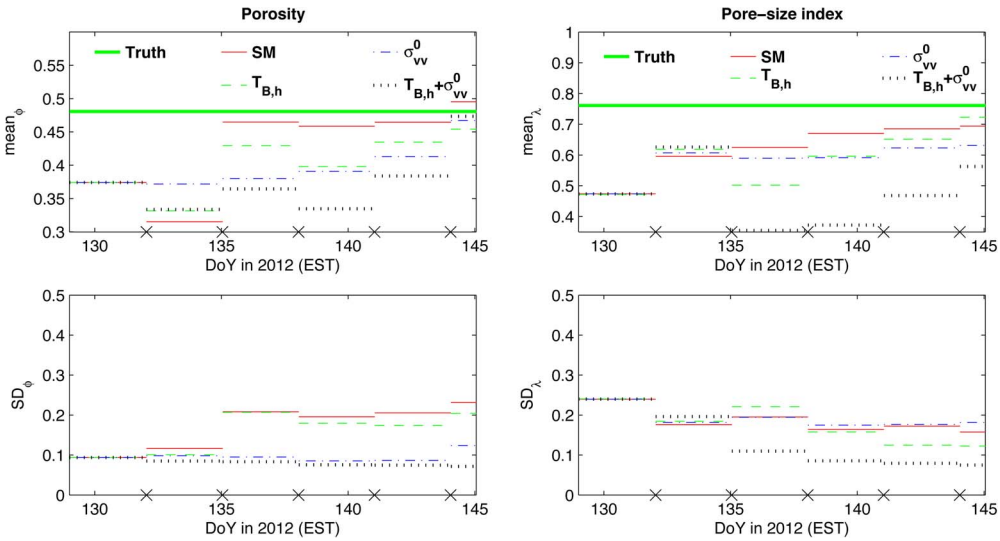

Fig. 3. Mean and standard deviation (SD) of the parameter estimates when assimilating synthetic observations of SM, passive, active, and AP and using the SSP.

that both bias correction methods predict SM estimates closer to the truth than the EnKF. The plots show that all assimilation algorithms reduce the differences between the estimates and the truth over time, improving the estimates in comparison with open-loop simulations, which depict an increasing difference over time. From DoY 129 to DoY 138, both the SSP and BCWF methods reached similar values of SM. After DoY 138, the BCWF obtained SM estimates closer to the truth. The lowest differences between the bias correction methods and the truth are obtained on DoYs 138 and 141.

Fig. 2(a) shows the bias estimated by the two bias correction methods when assimilating SM observations. For this figure, the open-loop bias is calculated by following (11) and the SM estimates from open loop. It is observed that the SM bias from SSP and BCWF always reduced compared with open loop. At the time of assimilation, the bias estimated by BCWF resulted in differences between SM estimates and the truth lower than 3.85% SM. As expected, this improvement reduced gradually during the propagation phase of the filter.

Fig. 3 presents the parameter values estimated for correcting the bias when assimilating SM observations and using the SSP method and their standard deviation (SD) over time. Porosity is the parameter that showed higher sensitivity than pore-size index to fix the difference between the SM estimates and the

SM observations. In contrast, pore-size index is the parameter with the lower SD.

2) Assimilation of Passive-Only, Active-Only, and AP Observations: Table IV summarizes the RMSE between the SM estimates, the ASD when assimilating H-pol passive, VV-pol active, and AP observations, and the time average bias (AB). The mean bias of 0.0324 m^3/m^3 introduced in SM resulted in a mean bias of 9.23 K in $T_{B,h}$ and of 1.01 dB in σ^0_{vv} for open-loop simulations. In general, when assimilating $T_{B,h}$, σ^0_{vv}, and $T_{B,h} + \sigma^0_{vv}$ observations and using the EnKF, the RMSE and the ASD for the SM estimates improved in comparison with open-loop simulations. In addition, the AB reduced when the bias correction methods were applied compared with open loop and EnKF.

When the bias corrections methods were applied, the SM estimates improved by 24%–44%, compared with the open loop, and by 10%–32%, compared with the EnKF. Similar to the assimilation of SM observations, during the assimilation of microwave passive, active, and AP observations, the lowest difference and ADs for the microwave estimates were obtained by the BCWF method.

Fig. 1(b)–(d) shows the time series between the truth and the estimates of the SM for open loop, the EnKF, and the two bias corrections methods (SSP and BCWF) when assimilating H-pol passive [see Fig. 1(b)], VV-pol active [see Fig. 1(c)], and AP [see Fig. 1(d)] observations. The two bias correction methods showed an improvement in the SM estimates compared with both open loop and EnKF. As shown in Fig. 1(b)–(d), the SM estimates are highly responsive to assimilation of $T_{B,h}$ and σ^0_{vv} observations and precipitations events. In all cases, the BCWF obtained SM estimates closer to the truth throughout the studied period.

When assimilating H-pol passive observations, improvements in the $T_{B,h}$ estimates of 10.20 K in average resulted in improvements of 39% in average in the SM, whereas the assimilation of VV-pol active observations resulted in improvements of 1.29 dB in average in σ^0_{vv} and of 40% in average in SM estimates (see Table IV). When assimilating simultaneous AP observations, combined improvements of 9.87 K in $T_{B,h}$ and 1.11 dB in σ^0_{vv} resulted in improvements of 38% in SM. From Table IV, it is observed that the bias correction methods obtained similar improvement in SM estimates when assimilating σ^0_{vv} or $T_{B,h}$ observations. This is a consequence of representing the bias effects as the addition of a constant value in the SM estimates at every single step. The addition of this constant value is equivalent to have a permanent water source in the system, resulting in reducing the sensitivity of passive observations to SM. In contrast, σ^0_{vv} is less sensitive to SM and then less affected by this representation. The BCWF obtained closer SM estimates than the SSP after DoY 135. The field in this study had a constant smooth surface over the studied period; thus, the plots in Fig. 1(b) show the response of passive observation to variations in SM only. The bias estimated by BCWF depicted a similar trend than that when assimilating SM observations [see Fig. 2(a) and (b)]. Similar to the assimilation of SM observations, porosity is more responsive than pore-size index to fix the bias when applying SSP (see Fig. 3).

During the assimilation of VV-pol active observations [see Fig. 1(c)], the maximum improvements were observed during the dry-down periods when the SM reached equilibrium or field capacity. The improvement when assimilating active observations is similar to assimilation of passive observations. In general, the BCWF obtained better estimates for both σ^0_{vv} and SM estimates than the SSP. The bias estimated by BCWF when assimilating active observations needed more points of assimilation before being close to the true value in comparison with passive observations [see Fig. 2(b) and (c)]. As observed in Fig. 2(c), when assimilating σ^0_{vv} observations, BCWF reduced the bias the most throughout the studied period. Similar to the bias estimation, when applying the SSP method to active observations, the updated parameters by the SSP method needed more points of assimilation before fixing the bias compared with the assimilation of passive observations (see Fig. 3).

When assimilating AP observations [see Fig. 1(d)], the SSP method resulted in SM estimates closer to the truth than those when assimilating passive-only or active-only observations [see Fig. 1(b)]. In contrast, the SM estimates from the BCWF were similar to active-only observations [see Fig. 1(c)], which were the closest estimates to the truth. Between the two bias correction methods, the BCWF obtained the lowest difference of SM in comparison with the truth. The BCWF combines all the uncertainty sources into the bias variable, and at each update, the posterior bias value is calculated considering only combined statistical information from the AP observations. In contrast, the SSP updates the SM sensitive parameters and accounts for their individual sensitivity to $T_{B,h}$ and σ^0_{vv} using the physics within the LSP-AP model during the propagation phase. However, once the maximum improvement was reached by compensating for the bias with a realistic value in the parameters, the SSP method kept the updated values of the parameters constant.

Overall, the BCWF showed to be the bias correction method that best fixed the bias when its effects are represented by adding a constant value in SM. Under real conditions, the uncertainties would be higher due to rougher surface conditions, vegetated terrains, or if the error in the model physics were known and the performance of the bias correction methods may be different.

B. Assimilation of $T_{B,h}$, σ^0_{vv}, and AP Observations From MicroWEX-11

In the previous sections, it was found that, when assimilating active and/or passive microwave observations, the lowest difference between the SM estimates and the truth was obtained by the BCWF and the lowest SD was given by the SSP. Assimilation of field observations, such as those from MicroWEX-11, provides insights into additional bias sources other than those from the forcings and parameters. As mentioned in Section VI-B, for the assimilation of MicroWEX-11 observations, the constant value added in the SM estimates within the LSP model during the synthetic experiment was removed. Table V shows the root-mean-square difference (RMSD) during the 15 days of the study, the time average difference (AD) between the SM estimates, and the field observations when

TABLE V
ROOT-MEAN-SQUARE DIFFERENCE (RMSD) BETWEEN THE TRUTH AND THE ESTIMATES OF NEAR-SURFACE SOIL MOISTURE (SM), RZSM, $T_{B,h}$, σ^0_{vv}, THEIR TIME AVERAGE BIAS (AB), AND THEIR ASSOCIATED AVERAGE STANDARD DEVIATION (ASD) WHEN USING BIAS CORRECTION METHODS AND ASSIMILATING MICROWEX-11 OBSERVATIONS. THE BIAS CORRECTION METHODS ARE THE SIMULTANEOUS STATE PARAMETER (SSP) UPDATE AND THE BIAS CORRECTION WITH FEEDBACK (BCWF) UPDATE

Scenario	Method	SM			$RZSM$			$T_{B,h}$		σ^0_{vv}	
		$RMSD$ $(vol\%)$	AB $(vol\%)$	ASD $(vol\%)$	$RMSD$ $(vol\%)$	AB $(vol\%)$	ASD $(vol\%)$	$RMSD$ (K)	ASD (K)	$RMSD$ (dB)	ASD (dB)
Open-loop		5.45	5.17	3.08	3.06	2.79	2.03	34.93	8.28	1.58	-27.10
SM	EnKF	3.56	2.99	2.40	0.59	0.21	1.05	—	—	—	—
	SSP	3.13	2.40	2.09	0.59	0.04	0.97	—	—	—	—
	BCWF	3.38	2.69	2.74	1.01	0.37	1.66	—	—	—	—
$T_{B,h}$	EnKF	3.40	2.72	2.44	0.75	0.16	1.04	35.68	7.63	—	—
	SSP	2.93	2.16	1.88	0.72	0.18	0.97	35.07	6.43	—	—
	BCWF	4.14	3.42	3.17	1.81	0.90	2.00	36.11	8.85	—	—
σ^0_{vv}	EnKF	4.06	3.60	2.55	1.23	1.08	1.20	—	—	1.98	-27.96
	SSP	3.85	3.36	2.08	1.25	1.09	1.15	—	—	2.08	-29.19
	BCWF	4.46	4.09	2.51	0.94	0.77	1.77	—	—	1.82	-28.44
$T_{B,h}$+σ^0_{vv}	EnKF	3.45	2.80	2.42	0.68	0.04	1.02	35.66	7.51	2.21	-28.21
	SSP	3.18	2.42	2.44	0.71	0.16	0.96	35.57	8.39	2.30	-28.18
	BCWF	4.21	3.57	3.32	1.64	0.97	2.02	36.00	9.58	2.07	-26.91

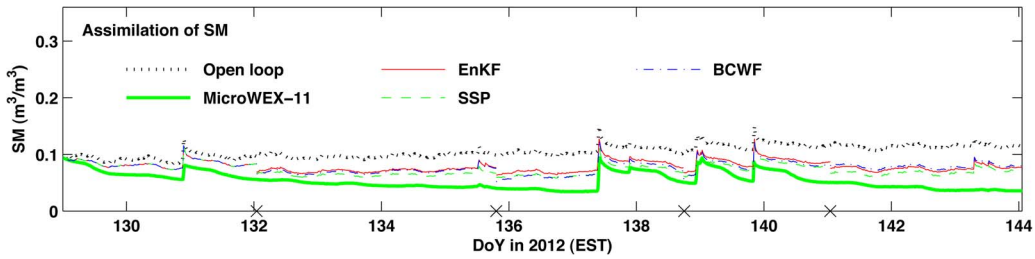

Fig. 4. Estimates of SM when assimilating MicroWEX-11 observations of SM and using the EnKF and the bias correction methods: SSP and BCWF.

assimilating SM, $T_{B,h}$, σ^0_{vv}, and $T_{B,h} + \sigma^0_{vv}$ observations using the standard EnKF, the SSP and BCWF methods, and the time average standard deviation (ASD). In general, the bias correction methods improved the SM compared with open loop and EnKF and reduced the difference between the SM estimates and MicroWEX-11 compared with both open loop and EnKF.

When assimilating SM observations, the EnKF improved the SM estimates by 38.5% in comparison with open loop. When the bias correction methods were applied, the SM estimates improved by 40%–45% in comparison with open loop and by 4%–11% in comparison with the EnKF. Among the two bias correction methods, the lowest RMSD in SM and the lowest AD in SM were obtained by the SSP method. Fig. 4 shows the time series of assimilation of MicroWEX-11 SM observations to estimate SM. The higher differences between the observations and the estimates occurred during precipitation events. During the dry-down periods (DoYs 131.5–137 and 140–144), at the time of the assimilation, the bias correction methods were closer to the observation with a difference lower than 0.0238 m^3/m^3. In general, the bias correction methods showed similar performance when assimilating either synthetic SM observations or MicroWEX-11 SM observations [see Figs. 1(a) and 4]. Fig. 8(a) shows the difference between the SM observations and the SM estimates from the two bias correction methods. The SSP obtained the lowest difference compared with open loop. During rainfall events, both bias correction methods obtained similar differences. The parameters estimated by the SSP also followed the trend showed by the synthetic experiment, and it was confirmed that porosity was the most sensitive soil parameter (see Fig. 9). This suggests that most of the sources of uncertainty in the field experiment come from the uncertainty in soil parameters.

Based on Table V, when assimilating $T_{B,h}$ observations, the EnKF and the SSP did not improve the $T_{B,h}$ estimates compared with the open loop, and the BCWF method increased the difference in the $T_{B,h}$ estimates. In general, the EnKF and the two bias correction methods obtained similar results to the open loop in estimating $T_{B,h}$ (see Table V). Unlike the lack of improvement in the RMSD in $T_{B,h}$, the ASD from the SSP method improved by 1.85 K in comparison with open loop. For the estimation of SM, the bias correction methods improved the estimates by 30%–50% compared with open loop. The SSP improved the SM estimates by 12% compared with EnKF. The SM estimates from the BCWF were similar to those from the EnKF. The lowest improvement was given by the BCWF method. Between the two bias correction methods, the SM estimates from SSP were closer to the observations. Fig. 5 shows the time series of both SM and $T_{B,h}$ estimates over the studied period. During the dry-down periods, the open loop underestimated the $T_{B,h}$ values but overestimated them by about 40 K immediately after the precipitation events. During the application of the assimilation methods, the SSP followed the trend more closely and the levels of both $T_{B,h}$ and SM observations. However, the $T_{B,h}$ estimates from the SSP methods did not reach as low values as the $T_{B,h}$ observations during the precipitation events. At the end of the assimilation period (DoYs 138–144), the SM estimates by the BCWF were similar to open loop.

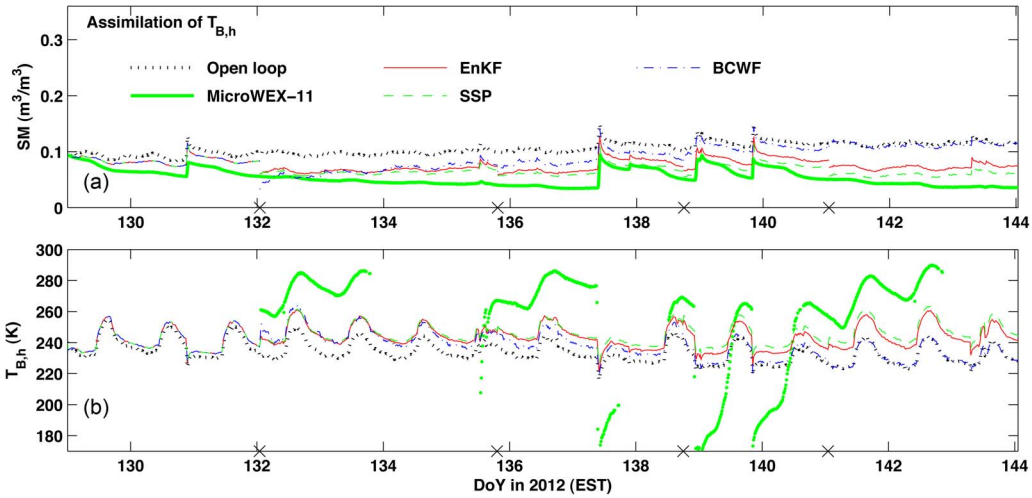

Fig. 5. Estimates of (a) SM and (b) $T_{B,h}$ when assimilating MicroWEX-11 observations of $T_{B,h}$ and using the EnKF and the bias correction methods: SSP and BCWF.

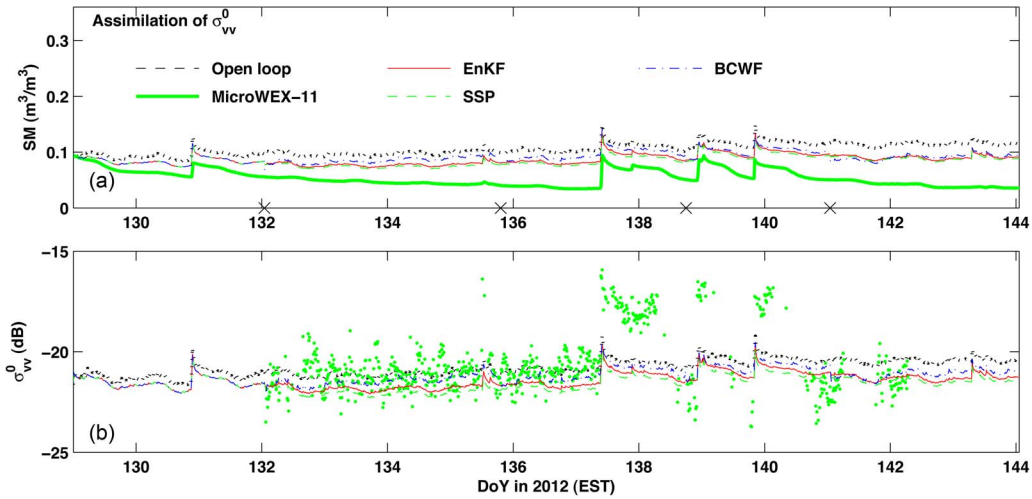

Fig. 6. Estimates of (a) SM and (b) σ^0_{vv} when assimilating MicroWEX-11 observations of σ^0_{vv} and using the EnKF and the bias correction methods: SSP and BCWF.

At the assimilation times of that period, the Kalman gain in the bias update equation [see (35)] was close to zero because of the low standard deviation in the bias estimated by the BCWF. Thus, the Kalman filter considered a case equivalent to the EnKF (bias-blind scenario). This indicates additional effects in the MicroWEX-11 observations that are not compensated by correcting the bias only in the SM estimates. These differences may come from roughness variations and contributions from the SM profile, particularly from the top layers [53]. The AP model did not reproduce the same behavior of the $T_{B,h}$ observed in the field due to imperfect biophysics in the estimation of the soil dielectric constant [21], [24]. It is observed that the AP model captures only the sensitivity of the passive observations during the dry-down periods. This suggests that improvements accounting for the SM profile need to be incorporated in the AP model to represent the sensitivity depicted by the observations [53]. Fig. 8(b) shows differences between SM observations and SM estimates by the bias correction methods compared with open loop when assimilating $T_{B,h}$ observations. It is observed that SSP corrected the difference the most.

When assimilating active observations, the EnKF did not improve the σ^0_{vv} estimates compared with open loop (see Table V). The EnKF and the bias correction methods obtained similar performance in improving σ^0_{vv}. The bias correction methods improved the SM by 20%–34% compared with open loop and by 0%–6% compared with EnKF (see Table V). For SM estimates, the lowest RMSD, the lowest AD, and the lowest ASD were given by the SSP method. Similar to the assimilation of $T_{B,h}$ observations, unlike the lack of improvement in σ^0_{vv}, there was an improvement in SM estimates. The assimilation of active observations confirms that there are other effects in MicroWEX-11 observations that cannot be compensated by correcting the bias only in SM. Fig. 6 shows the time series of both SM and σ^0_{vv} estimates over the studied period. It is observed that, from DoY 132 to DoY 137.5, although σ^0_{vv} estimates from open loop were close to σ^0_{vv} observations, SM estimates from open loop were higher than SM observations. From DoY 140 to DoY 142, σ^0_{vv} estimates were higher than observations, and the bias correction methods improved the σ^0_{vv} estimates. During the precipitation events (DoYs 137–140), the

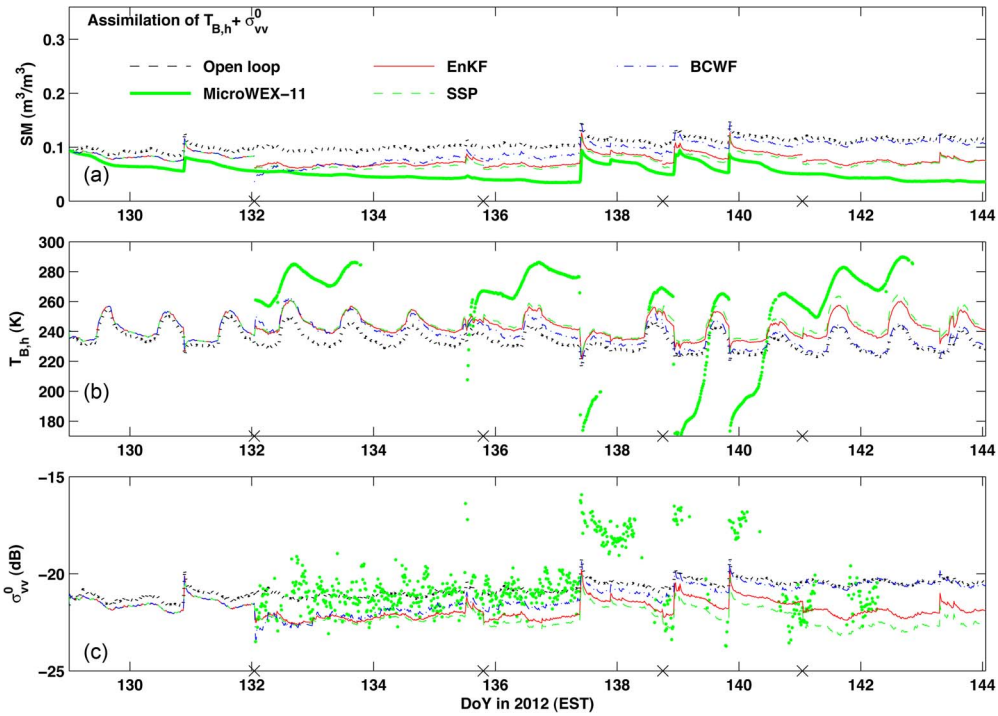

Fig. 7. Estimates of (a) SM, (b) $T_{B,h}$, and (c) σ^0_{vv} when assimilating MicroWEX-11 observations of simultaneous $T_{B,h}$ and σ^0_{vv} and using the EnKF and the bias correction methods: SSP and BCWF.

MicroWEX-11 active observations depicted high values that the AP model could not reproduce. This resulted in σ^0_{vv} and SM estimates close to open loop during rainfalls, even after applying the bias correction methods. When the bias correction methods were applied close to rainfalls, the statistics within the Kalman gain indicated that, to compensate the difference between the active observations and the σ^0_{vv} estimates, the SM values needed to be increased. This resulted in posterior SM values higher than prior values, producing a gradual increase in the difference between the SM observations and the SM estimates. The difference between the observations and estimates of σ^0_{vv} may come from roughness variations and contributions from soil volume scattering. The main contribution in the field backscatter signal comes from volume scattering for SM values lower than 0.05 m^3/m^3; in contrast, the main contribution comes from surface scattering for SM values higher than 0.05 m^3/m^3 [50]. Since the IEM accounts only for surface scattering, its active and passive estimates do not reproduce high variations as those depicted by MicroWEX-11 observations, particularly during rainy periods. Figs. 8(c) and 9 show the difference between the bias correction methods and MicroWEX-11 observations and the parameter values estimated by the SSP, respectively. In both figures, the low sensitivity of σ^0_{vv} to soil parameters is confirmed. The SM bias estimated (see Fig. 8) is similar to the initial values, and the update values for ϕ and λ by the SSP in Fig. 9 are marginally modified in comparison with the initial values. Fig. 8(c) shows the difference between the SM estimates from the bias correction methods and the MicroWEX-11 SM observations when assimilating σ^0_{vv} observations. It is observed that the difference in SM was higher when assimilating active observations than passive observations.

When assimilating simultaneous AP observations, the EnKF and the bias correction methods performed similar to the scenario of assimilation of passive-only observations but better than during the assimilation of active-only observations. In the AP scenario, the EnKF and the bias correction methods did not improve the σ^0_{vv} and $T_{B,h}$ estimates compared with open loop (see Table V). Unlike the lack of improvement in the microwave estimates, the EnKF improved the SM estimates by 41% compared with open loop (see Table V). The bias correction methods improved the SM estimates by 30%–45% compared with open loop and by 0%–7% in comparison with EnKF. The BCWF predicted values similar to the EnKF (see Table V) and similar to the passive-only assimilation case. The highest improvement was given by the SSP method. Fig. 7 shows the time series of the estimates of SM, $T_{B,h}$, and σ^0_{vv}. The two bias correction methods tried to follow closer the trend and the levels of both $T_{B,h}$ and σ^0_{vv} observations. Similar to the assimilation of $T_{B,h}$ observations, the SSP and the EnKF obtained similar estimates of SM after DoY 138, primarily because of the low value of the Kalman gain in the bias update equation. During the precipitation events, the estimates from the methods did not reach as low values as the $T_{B,h}$ observations, and the σ^0_{vv} did not reach as high values as the σ^0_{vv} observations. Due to these drawbacks in the AP model, during the rainy periods, the AP observations provided opposite information to the bias corrections methods. While $T_{B,h}$ and σ^0_{vv} indicated an increment in SM, the SM values overestimated the SM observations. This opposite information resulted in low improvement in SM by the bias correction methods. Fig. 8 shows the bias estimated by the BCWF. It is observed that the trend depicted by the assimilation of AP is similar to that by the assimilation of SM and $T_{B,h}$ observations. In Fig. 9,

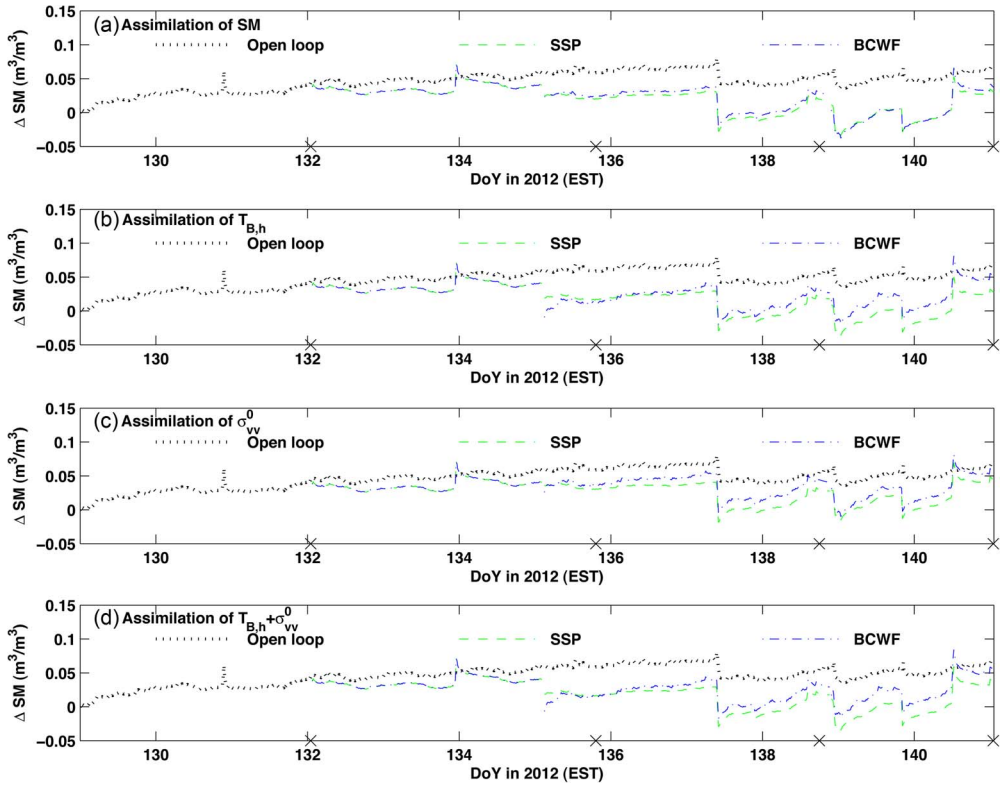

Fig. 8. Estimates of bias in SM when assimilating MicroWEX-11 observations of SM, passive, active, and AP and using the EnKF and the bias correction methods: SSP and BCWF.

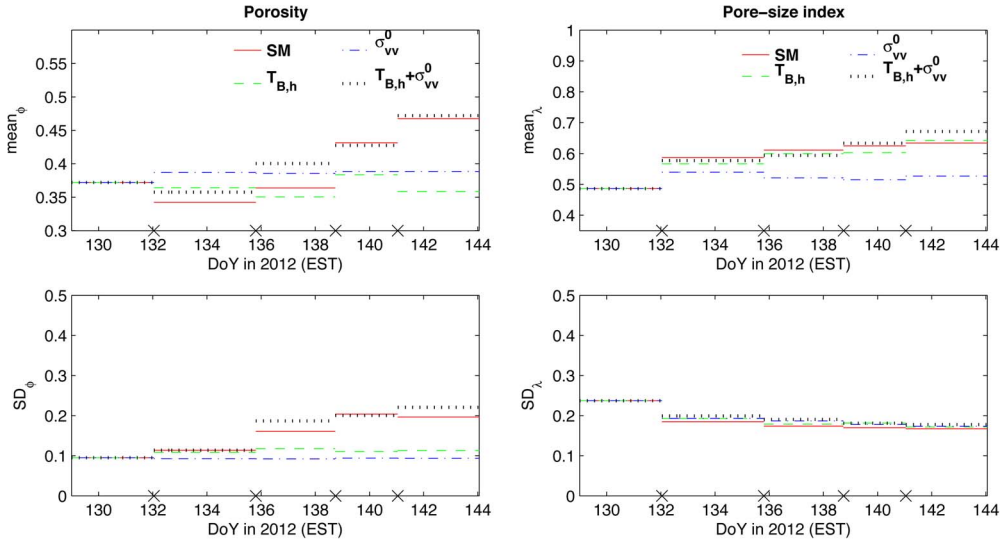

Fig. 9. Mean and standard deviation (SD) of the parameter estimates when assimilating MicroWEX-11 observations of SM, passive, active, and AP and using the SSP.

we plot the updated values for porosity and pore-size index by the SSP. Porosity estimates had a trend similar to those from the assimilation of SM estimates and had higher values than the assimilation of passive-only and active-only observations. Pore-size index estimates from the assimilation of AP observations were closer to the estimates from the assimilation of SM and $T_{B,h}$ observations.

In general, the bias correction methods improved the SM estimates when assimilating either synthetic or MicroWEX-11 observations. Unlike the synthetic study, for the assimilation of field microwave observations, the lowest difference between the estimates and the observations was obtained by the SSP. The reduction in the performance showed by the bias correction methods in improving the SM estimates, in comparison with the synthetic case, showed the importance of incorporating new representations to account for the SM profile in the estimation of $T_{B,h}$ and soil scattering models considering both surface and volume contributions in the estimation of σ^0_{vv}.

When correcting the bias in an assimilation framework, observations of $T_{B,h}$ with an uncertainty of 4 K and observations of σ^0_{vv} with an uncertainty of 1 dB obtained SM estimates with an RMSE ranging between 0.0293 and 0.0414 m^3/m^3. The sensor on board the SMOS and the SMAP reported an accuracy from 1.3 to 2.6 K [6], [7] for passive observations and an accuracy of 0.5 dB [7] for active observations. Based on the methodology presented in this paper and the accuracy reported in the SMOS and SMAP missions, it is expected to reduce the uncertainty in SM reported in Table V.

VIII. Summary and Conclusions

In this paper, two bias correction approaches for nonlinear observation operators using an EnKF framework have been investigated: an online bias correction algorithm with feedback (BCWF) and a simultaneous state parameter (SSP) update. New equations for correcting the bias in the BCWF approach were derived for cases of nonlinear observation operators following [37] and [38] because current versions of this approach were not applicable for improving SM by assimilating microwave observations. EnKF-based bias correction algorithms were used to assimilate synthetic and field passive and/or active microwave observations at L-band to improve the SM estimates. In the synthetic study, a constant value was added in the SM estimates to generate the bias within the LSP model. The sources of uncertainties were the soil parameters in the LSP model and all forcings. In addition, an observation error with zero mean and a standard deviation of 4 K in $T_{B,h}$ and 1 dB in σ^0_{vv} were considered. The impact of the bias correction methods in improving SM estimates was analyzed by applying the SSP and BCWF approaches. In general, the bias correction methods resulted in SM estimates closer to the true values than the standard EnKF for both synthetic and field observations.

The two approaches resulted in closer estimates of SM to observations; the lowest RMSE was obtained by BCWF for the SM estimates when assimilating active/passive synthetic microwave observations. While the BCWF compensates for the bias by correcting the posterior state estimates with the updated bias estimates, the SSP compensates for the bias by modifying the parameter values of the ensemble. The improvement in the SM estimates by the bias correction methods was 32%–48% in comparison with open loop and 10%–32% in comparison with EnKF for microwave synthetic observations. As expected, the assimilation of $T_{B,h}$ observations resulted in estimates that were closer to the true values of SM than the assimilation of σ^0_{vv} observations, as the active observations are highly influenced by the uncertainty in the surface roughness of 2.5 cm. The assimilation of AP observations showed better performance than the assimilation of passive-only observations and similar performance to assimilation of active-only observations. This is a consequence of representing the bias effects by including a constant value at every single step in the SM estimates from LSP during the synthetic experiment.

In comparison with synthetic observations, the assimilation of MicroWEX-11 active/passive observations suggests other sources of uncertainty than those in forcings and model parameters. For the assimilation of field microwave observations, the lowest RMSD between the estimates and the observations was obtained by the SSP over the full studied period. In general, the lowest ASD was also obtained by the SSP method. During the assimilation of passive-only observations, higher differences of 10–15 K were produced during and immediately following the precipitation/irrigation events. It was found that $T_{B,h}$ was underestimated during dry-down periods and overestimated during precipitation events, compared with the observations due to the equations used to relate the soil dielectric constant and SM. During the assimilation of active-only observations, the SSP showed the closest trend to σ^0_{vv} observations. The difference between the observations and σ^0_{vv} estimates from the bias correction methods may come from roughness variations and contributions from volume scattering. The AP provided values of σ^0_{vv} close to the MicroWEX-11 observations all over the studied period. When assimilating AP observations, due to the drawbacks in the AP model, the active/passive observations provided conflicting information regarding the SM observations to the bias corrections methods during rainfall events. While $T_{B,h}$ and σ^0_{vv} indicated an increment in SM, the SM observations indicated a decrement in the SM estimates. This contradictory information resulted in low improvement by the bias correction methods. However, among the different scenarios, the assimilation of AP observations showed the best performance in improving SM estimates. Based on the differences between the assimilation of synthetic and MicroWEX-11 observations, it is highly recommended to incorporate new representations to account for the SM profile in the estimation of $T_{B,h}$ and soil scattering models considering both surface and volume contributions in the estimation of σ^0_{vv}.

Based on the methodology presented in this paper and the accuracy reported in the SMOS and SMAP missions, it is expected to obtain SM estimates with errors lower than 0.04 m^3/m^3 when correcting the bias in an assimilation framework.

Acknowledgment

The authors would like to thank the University of Florida High-Performance Computing Center for the computational resources and support provided for all model simulations conducted in this study. The authors would also like to thank the anonymous reviewers for their interesting comments and suggestions that have contributed in improving the quality of this paper.

References

[1] J. Judge, L. Abriola, and A. England, "Numerical validation of the land surface process component of an LSP/R model," *Adv. Water Res.*, vol. 26, no. 7, pp. 733–746, Jul. 2003.

[2] W. Crow and E. Wood, "The assimilation of remotely sensed soil brightness temperature imagery into a land surface model using ensemble Kalman filtering: A case study based on ESTAR measurements during SGP97," *Adv. Water Res.*, vol. 26, no. 2, pp. 137–149, Feb. 2003.

[3] R. H. Reichle, J. P. Walker, R. D. Koster, and P. R. Houser, "Extended versus ensemble Kalman filter for land data assimilation," *J. Hydrometeorol.*, vol. 3, no. 6, pp. 728–740, Dec. 2002.

[4] R. H. Reichle, D. B. McLaughlin, and D. Entekhabi, "Hydrologic data assimilation with the ensemble Kalman filter," *Mon. Weather Rev.*, vol. 130, no. 1, pp. 103–114, Jan. 2002.

[5] E. Burke, W. Shuttleworth, K. Lee, and L. Bastidas, "Using area-average remotely sensed surface soil moisture in multipatch land data assimilation systems," *IEEE Trans. Geosci. Remote Sens.*, vol. 39, no. 10, pp. 2091–2100, Oct. 2001.

[6] Y. Kerr *et al.*, "The SMOS mission: New tool for monitoring key elements of the global water cycle," *Proc. IEEE*, vol. 98, no. 5, pp. 666–687, May 2010.

[7] D. Entekhabi *et al.*, "The Soil Moisture Active Passive (SMAP) mission," *Proc. IEEE*, vol. 98, no. 5, pp. 704–716, May 2010.

[8] A. T. Joseph, R. van der Velde, P. E. O'Neill, R. H. Lang, and T. Gish, "Soil moisture retrieval during a corn growth cycle using L-band (1.6 GHz) radar observations," *IEEE Trans. Geosci. Remote Sens.*, vol. 46, no. 8, pp. 2365–2374, Aug. 2008.

[9] S. C. Dunne and D. Entekhabi, "Land surface state and flux estimation using the ensemble Kalman smoother during the Southern Great Plains 1997 field experiment," *Water Res. Res.*, vol. 42, no. 1, Jan. 2006, Art. ID. W01407.

[10] D. P. Thoma *et al.*, "Comparison of four models to determine surface soil moisture from C-band radar imagery in a sparsely vegetated semiarid landscape," *Water Res. Res.*, vol. 42, no. 1, Jan. 2006, Art. ID. W01418.

[11] S. Paloscia, P. Pampaloni, S. Pettinato, P. Poggi, and E. Santi, "The retrieval of soil moisture from ENVISAT/ASAR data," in *Proc. EARSel eProc.*, 2005, vol. 4, pp. 44–51.

[12] I. J. Davenport, J. Fernandez-Galvez, and R. J. Gurney, "A sensitivity analysis of soil moisture retrieval from the tau-omega microwave emission model," *IEEE Trans. Geosci. Remote Sens.*, vol. 43, no. 6, pp. 1304–1316, Jun. 2005.

[13] W. Crow, "Correcting land surface model predictions for the impact of temporally sparse rainfall rate measurements using an ensemble Kalman filter and surface brightness temperature observations," *J. Hydrol.*, vol. 4, no. 5, pp. 960–973, Oct. 2003.

[14] W. L. Crosson, C. A. Laymon, R. Inguva, and C. Bowman, "Comparison of two microwave radiobrightness models and validation with field measurements," *IEEE Trans. Geosci. Remote Sens.*, vol. 40, no. 1, pp. 143–152, Jan. 2002.

[15] M. Moghaddam, S. Saatchi, and R. Cuenca, "Estimating subcanopy soil moisture with radar," *J. Geophys. Res.*, vol. 105, no. D11, pp. 14 899–14 911, Jun. 2000.

[16] N. S. Chauhan, "Soil moisture estimation under a vegetation cover: Combined active passive microwave remote sensing approach," *Int. J. Remote Sens.*, vol. 18, no. 5, pp. 1079–1097, Mar. 1997.

[17] P. E. O'Neill, N. Chauhan, and T. Jackson, "Use of active and passive microwave remote sensing for soil moisture estimation through corn," *Int. J. Remote Sens.*, vol. 17, no. 10, pp. 1851–1865, Jul. 1996.

[18] P. C. Dubois, J. van Zyl, and T. Engman, "Measuring soil moisture with imaging radars," *IEEE Trans. Geosci. Remote Sens.*, vol. 33, no. 4, pp. 915–926, Jul. 1995.

[19] Y. Oh, K. Sarabandi, and F. T. Ulaby, "An empirical model and an inversion technique for radar scattering from bare soil surfaces," *IEEE Trans. Geosci. Remote Sens.*, vol. 30, no. 2, pp. 370–381, Mar. 1992.

[20] Y. Du, F. T. Ulaby, and M. C. Dobson, "Sensitivity to soil moisture by active and passive microwave sensors," *IEEE Trans. Geosci. Remote Sens.*, vol. 38, no. 1, pp. 105–114, Jan. 2000.

[21] K. Nagarajan, J. Judge, A. Monsivais-Huertero, and W. D. Graham, "Impact of assimilating passive microwave observations on root-zone soil moisture under dynamic vegetation conditions," *IEEE Trans. Geosci. Remote Sens.*, vol. 50, no. 11, pp. 4279–4291, Nov. 2012.

[22] S. C. Dunne, D. Entekhabi, and E. G. Njoku, "Impact of multiresolution active and passive microwave measurements on soil moisture estimation using the ensemble Kalman smoother," *IEEE Trans. Geosci. Remote Sens.*, vol. 45, no. 4, pp. 1016–1028, Apr. 2007.

[23] A. K. Fung, Z. Li, and K. S. Chen, "Backscattering from a randomly rough dielectric surface," *IEEE Trans. Geosci. Remote Sens.*, vol. 30, no. 2, pp. 356–369, Mar. 1992.

[24] T. D. Wu, K. Chen, and J. Shi, "A study of an AIEM model for bistatic scattering from randomly rough surfaces," *IEEE Trans. Geosci. Remote Sens.*, vol. 46, no. 9, pp. 2584–2598, Sep. 2008.

[25] M. A. Fung, *Microwave Scattering and Emission Models and Applications*. Norwood MA, USA: Artech House, 1994.

[26] K. S. Chen *et al.*, "Emission of rough surfaces calculated by the integral equation method with comparison to three-dimensional moment method simulations," *IEEE Trans. Geosci. Remote Sens.*, vol. 41, no. 1, pp. 90–101, Jan. 2003.

[27] C. Huang, X. Li, L. Lu, and J. Gu, "Experiments of one-dimensional soil moisture assimilation system based on ensemble Kalman filter," *Remote Sens. Environ.*, vol. 112, no. 3, pp. 888–900, Mar. 2008.

[28] A. Monsivais-Huertero, W. D. Graham, J. Judge, and D. Agrawal, "Effect of simultaneous state-parameter estimation and forcing uncertainties on root-zone soil moisture for dynamic vegetation using EnKF," *Adv. Water Res.*, vol. 33, no. 4, pp. 468–484, Apr. 2010.

[29] W. Crow, W. P. Kustas, and J. H. Prueger, "Monitoring root-zone soil moisture through the assimilation of a thermal remote sensing-based soil moisture proxy into a water balance model," *Remote Sens. Environ.*, vol. 112, no. 4, pp. 1268–1281, Apr. 2008.

[30] V. R. N. Pauwels *et al.*, "Optimization of a coupled hydrology-crop growth model through the assimilation of observed soil moisture and leaf area index using an ensemble Kalman filter," *Water Res. Res.*, vol. 43, no. 4, Apr. 2007, Art. ID. W04421.

[31] H. Moradkhani, S. Sorooshian, H. V. Gupta, and P. R. Houser, "Dual state-parameter estimation of hydrological models using ensemble Kalman filter," *Adv. Water Res.*, vol. 28, no. 2, pp. 135–147, Feb. 2005.

[32] W. Margulis, D. McLaughlin, D. Entekhabi, and S. Dunne, "Land data assimilation and estimation of soil moisture using measurements from the Southern Great Plains 1997 field experiment," *Water Res. Res.*, vol. 38, no. 12, pp. 35-1–35-18, Dec. 2002.

[33] R. H. Reichle and R. D. Koster, "Bias reduction in short records of satellite soil moisture," *Geophys. Res. Lett.*, vol. 31, no. 19, Oct. 2004, Art. ID. L19501.

[34] A. Lorenc and O. Hammon, "Objective quality control of observations using Bayesian methods: Theory, and a practical implementation," *Q. J. R. Meteorol. Soc.*, vol. 114, no. 480, pp. 515–543, Jan. 1988.

[35] D. Ryu, W. T. Crow, X. Zhan, and T. J. Jackson, "Correcting unintended perturbation biases in hydrologic data assimilation," *J. Hydrometeorol.*, vol. 10, no. 3, pp. 734–750, Jun. 2009.

[36] G. J. M. De Lannoy, P. R. Houser, V. R. N. Pauwels, and N. E. C. Verhoest, "State and bias estimation for soil moisture profiles by an ensemble Kalman filter: Effect of assimilation depth and frequency," *Water Res. Res.*, vol. 43, no. 6, Jun. 2007, Art. ID. W06401.

[37] B. Friedland, "Treatment of bias in recursive filtering," *IEEE Trans. Autom. Control*, vol. 14, no. 4, pp. 359–367, Aug. 1969.

[38] D. Dee and A. Da Silva, "Data assimilation in the presence of forecast bias," *Q. J. R. Meteorol. Soc.*, vol. 124, no. 545, pp. 269–295, Jan. 1998.

[39] G. J. M. De Lannoy, R. H. Reichle, P. R. Houser, V. R. N. Pauwels, and N. E. C. Verhoest, "Correcting for forecast bias in soil moisture assimilation with the ensemble Kalman filter," *Water Res. Res.*, vol. 43, no. 9, Sep. 2007, Art. ID. W09410.

[40] J. Judge, A. W. England, J. R. Metcalfe, D. McNichol, and B. E. Goodison, "Calibration of an integrated Land Surface Process and Radiobrightness (LSP/R) model during summertime," *Adv. Water Res.*, vol. 31, no. 1, pp. 189–202, Jan. 2008.

[41] S. Verseghy, N. McFarlane, and M. Lazare, "CLASS—A Canadian land surface scheme for GCMs, II. vegetation model and coupled runs," *Int. J. Climatol.*, vol. 13, no. 4, pp. 347–370, May/Jun. 1993.

[42] J. Peixoto and A. Oort, *Physics of Climate*. New York, NY, USA: AIP, 1992.

[43] J. Philip and D. de Vries, "Moisture movement in porous materials under temperature gradients," *Trans. Amer. Geophys. Union*, vol. 38, no. 2, pp. 222–232, Apr. 1957.

[44] D. de Vries, "Simultaneous transfer of heat and moisture in porous media," *Trans. Am. Geophys. Union*, vol. 39, no. 5, pp. 909–916, Oct. 1958.

[45] J. Casanova and J. Judge, "Estimation of energy and moisture fluxes for dynamic vegetation using coupled SVAT and crop-growth models," *Water Res. Res.*, vol. 44, no. 7, Jul. 2008, Art. ID. W07415.

[46] F. Ulaby, R. More, and A. Fung, *Microwave Remote Sensing: Active and Passive*, vol. I. Boston, MA, USA: Artech House, 1981.

[47] A. Gelb, *Applied Optimal Estimation*. Cambridge, MA, USA: MIT Press, 1974.

[48] G. Evensen, "The ensemble Kalman filter: Theoretical formulation and practical implementation," *Ocean Dynam.*, vol. 53, no. 4, pp. 343–367, Nov. 2003.

[49] V. L. Mironov, M. C. Dobson, V. H. Kaupp, S. A. Komarov, and V. N. Kleshchenko, "Generalized refractive mixing dielectric model for moist soils," *IEEE Trans. Geosci. Remote Sens.*, vol. 42, no. 4, pp. 773–785, Apr. 2004.

[50] P. Liu, "Integration of active and passive microwave signatures characterization of soil properties," Ph.D. dissertation, Dept. Agricult. and Biol. Eng., Univ. Florida, Gainesville, FL, USA, Mar. 2013.

[51] G. J. Ciach, "Local random errors in tipping-bucket rain gauge measurements," *J. Atmos. Ocean. Technol.*, vol. 20, no. 5, pp. 752–759, May 2003.

[52] E. Habib, W. F. Krajewski, and A. Kruger, "Sampling errors of tipping-bucket rain gauge measurements," *J. Hydrol. Eng.*, vol. 6, no. 2, pp. 159–166, Apr. 2001.

[53] P. Liu, R. D. Roo, A. England, and J. Judge, "Impact of moisture distribution within the sensing depth on L- and C- band emission in sandy soils," *IEEE J. Sel. Topics Appl. Earth Observ. Remote Sens.*, vol. 6, no. 2, pp. 887–889, Apr. 2012.
[54] J. Goudriaan, *Crop Micrometeorology: A Simulation Study*. 1st ed. Wageningen, The Netherlands: Centre for Agricultural Publishing and Documentation, 1977.
[55] C. Rossi and J. R. Nimmo, "Modeling of soil water retention from saturation to oven dryness," *Water Res. Res.*, vol. 30, no. 3, pp. 701–708, 1994.

Alejandro Monsivais-Huertero (S'06–M'07–SM'13) received the B.S. degree in telecommunications engineering from the National Autonomous University of Mexico, Mexico City, Mexico, in 2002 and the M.S. degree in microwaves and optical telecommunications and the Ph.D. degree in microwaves, electromagnetism, and optoelectronics from the University of Toulouse, Toulouse, France, in 2004 and 2007, respectively.

From 2004 to 2006 and from 2006 to 2007, he was with the Antennes, Dispositifs et Matériaux Microondes Laboratory and the Laboratoire d'Etudes et de Recherche en Imagerie Spatiale et Médicale, respectively, both at the University of Toulouse. From 2008 to 2009, he was a Postdoctorate Research Associate with the Center for Remote Sensing, Department of Agricultural and Biological Engineering, University of Florida, Gainesville, FL, USA. Since 2010, he has been a Researcher with the Superior School of Mechanical and Electrical Engineering campus Ticoman of the National Polytechnic Institute of Mexico, Mexico City. His research areas of interest are in microwave and millimeter-wave radar remote sensing, electromagnetic wave propagation, and retrieval algorithms.

Jasmeet Judge (S'94–M'00–SM'05) received the Ph.D. degree in electrical engineering and atmospheric, oceanic, and space sciences from the University of Michigan, Ann Arbor, MI, USA, in 1999.

She is currently the Director of the Center for Remote Sensing and an Associate Professor in the Department of Agricultural and Biological Engineering in the Institute of Food and Agricultural Sciences with the University of Florida, Gainesville, FL, USA. Her research interests are in microwave remote sensing applications to terrestrial hydrology for dynamic vegetation, data assimilation, modeling of energy and moisture interactions at the land surface and in the vadose zone, and spatiotemporal scaling of remotely sensed observations in heterogenous landscapes.

Dr. Judge is the Chair of the National Academies' Committee on Radio Frequencies and a member of the Frequency Allocations in Remote Sensing Technical Committee in the IEEE Geoscience and Remote Sensing Society. She has also served the American Geophysical Union as a Chair of the Remote Sensing Technical Committee in the Hydrology Section.

Susan Steele-Dunne received the S.M. and Ph.D. degrees in hydrology from the Massachusetts Institute of Technology, Cambridge, MA, USA, in 2002 and 2006, respectively.

Since 2008, she has been with the Water Resources Section, Faculty of Civil Engineering and Geosciences, Delft University of Technology, Delft, The Netherlands. Her research interests include remote sensing, data assimilation, land–atmosphere interactions, and land surface modeling.

Dr. Steele-Dunne is a member of the American Meteorological Society and the American Geophysical Union. She has also served the American Geophysical Union Hydrology Section as a member of the Remote Sensing Technical Committee and the Hydrological Sciences Award committee and the American Meteorological Society as a member of the Hydrology Committee.

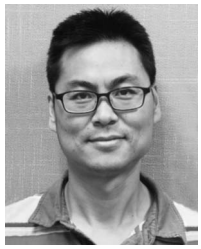

Pang-Wei Liu (S'09–M'13) received the Ph.D. degree in agricultural engineering, with a minor in electrical engineering, from the University of Florida, Gainesville, FL, USA, in 2013.

He is currently a Postdoctoral Research Associate with the Center for Remote Sensing, Institute of Food and Agricultural Sciences, University of Florida. His research interests include application of LiDAR for forest biomass, active and passive microwave remote sensing modeling for soil moisture and agricultural crops under dynamic vegetation conditions, data assimilation with crop growth models, and Global Navigation Satellite System (GNSS) remote sensing for terrestrial applications.

Dr. Liu is a member of the IEEE Geoscience and Remote Sensing Society and the American Geophysical Union.